Plasma Sources
Science and
Technology

PAPER • **OPEN ACCESS**

Comparison of fluid and particle-in-cell 3D simulations of negative streamers in CO_2 with admixtures of C_4F_7N

To cite this article: Thomas J G Smits *et al* 2026 *Plasma Sources Sci. Technol.* **35** 045005

Plasma Sources Science and Technology

OPEN ACCESS

RECEIVED
7 October 2025

REVISED
17 February 2026

ACCEPTED FOR PUBLICATION
12 March 2026

PUBLISHED
7 April 2026

PAPER

Comparison of fluid and particle-in-cell 3D simulations of negative streamers in CO_2 with admixtures of C_4F_7N

Thomas J G Smits[1,*], **Jannis Teunissen**[1,3] and **Ute Ebert**[1,2]

[1] Centrum Wiskunde & Informatica, Amsterdam, The Netherlands
[2] Eindhoven University of Technology, Eindhoven, The Netherlands
[3] Centre for mathematical Plasma Astrophysics, KU Leuven, Belgium
[*] Author to whom any correspondence should be addressed.

E-mail: thomas.smits@cwi.nl

Keywords: negative streamer discharges, fluid and particle models, transport and reaction coefficients, 3D modelling, insulation gas, mixtures of CO_2 with C_4F_7N

Abstract

CO_2 with an admixture of C_4F_7N could serve as an eco-friendly alternative to the extreme greenhouse gas SF_6 in high-voltage insulation. Streamer discharges in such gases are different from those in air due to the rapid conductivity decay in the streamer channels. Furthermore, since no effective photoionisation mechanism is known, we expect discharge growth to be more stochastic than in air. In this paper we investigate whether conventional fluid models provide an good approximation to a particle-in-cell model for negative streamers in CO_2 with admixtures of 1 or 10% C_4F_7N Higher fractions were not included, as C_4F_7N admixtures in high-voltage insulation rarely exceed 10% C_4F_7N. We focus on 3D simulations of negative streamers. First we review cross section databases for C_4F_7N and CO_2. Then we compare a two-term Boltzmann solver with a Monte Carlo method to compute reaction and transport coefficients from the cross sections. Afterwards we compare 3D fluid simulations with the local field (LFA) or local energy approximation (LEA) against particle simulations. In general, we find that the results of particle and fluid models are quite similar. One difference we observe is that particle simulations are intrinsically stochastic, leading to more branching. Furthermore, the LEA model does not show better agreement with the particle simulations than the LFA model. We also discuss the effect and choice of different boundary conditions on the negative rod electrode.

1. Introduction

1.1. Streamers in air and in new insulation gases

Streamers are ionisation fronts with strong local field enhancement. They frequently determine the initial stage of electrical breakdown of gases [1]. Streamers in air are the most widely investigated, but their behaviour does not seem to be generic for other gases because of the strong photoionisation mechanism in air. In this study, we analyse simulations of negative streamers in mixtures of CO_2 with C_4F_7N (abbreviated as CFN), which is an eco-friendly insulation gas [2].

SF_6 is used as an insulation gas in many high-voltage applications, but it is the most potent greenhouse gas [3, 4]. Hence, SF_6 urgently needs to be replaced. The large electron attachment coefficient and, therefore the high critical field make CFN-CO_2 mixtures suitable candidates for high-voltage insulation. However, streamer discharges in eco-friendly alternatives differ significantly from those in air, as shown in [5] for C5-Fluoroketone with air. Similar behaviour has been observed in [6] and in [7] for CO_2 with admixtures of CFN. On the microscopic level, these gases have high attachment rates and an unknown mechanism of photoionisation. On the macroscopic level, the discharges in the insulation gases do not form long conducting streamer channels. Instead, there are isolated streamer heads that only propagate if the background field is close to the critical field [6]. These macro- and microscopic properties differ significantly from discharges in air.

Another distinction lies in the propagation of positive versus negative streamers. Negative streamers have a negatively charged layer of electrons around their head, and they propagate against the electric field. Electrons are accelerated away from the streamer, so no external source of free electrons ahead of the streamer is needed. In contrast, positive streamers have a positively charged layer at their head and move along the electric field. Electrons are accelerated toward them, requiring a source of free electrons ahead of the streamer for propagation [1]. Therefore, negative streamers can propagate in any gas, but the existence of positive streamers depends on a source of free electrons. For air photoionisation provides such a source, but in most other gases such a mechanism is unknown.

In [8] it was observed that negative CO_2 streamers were faster than positive streamers in strongly non-uniform background fields. We expect similar behaviour in CO_2 with an admixture of CFN, when CO_2 is the main component. It is unclear if efficient free electron sources exist in CO_2 with CFN admixtures. If not, is it difficult for positive streamers to propagate, and we expect negative streamers to propagate more easily. This would be opposite to the situation in air, in which positive streamers are dominant [1].

1.2. Publications on 2D cylindrical fluid simulations with CFN admixtures

Streamer discharges are commonly simulated with a fluid model using the local field approximation (LFA). The LFA assumes that electrons instantaneously relax to the local field, so that transport and reaction coefficients are functions of the local electric field. Studies of axisymmetric streamers in CO_2 with admixtures of CFN using fluid models and the LFA have been presented in [9–14].

If electrons pass through a rapidly changing electric field, the validity of the LFA is questionable. An improvement of this classical approximation is the local energy approximation (LEA), in which transport and reaction coefficients are functions of the local mean electron energy. Examples in which an LEA is required are given in [15, 16]. While the LFA includes one reaction-drift-diffusion equation for the electron density, the LEA requires an additional reaction-drift-diffusion equation for the mean electron energy. LFA and LEA can be derived from the velocity moments of the Boltzmann equation with a truncation of the expansion after the first or second term [17, 18]. Fewer studies have used the LEA; a study of N_2 with an admixture of CFN has been published in [19].

Many authors have used 2D cylindrical fluid models to simulate discharges in gases with admixtures of CFN [9–14, 19]. These models have been used to study the influence of different electrode shapes [11] or the characteristics of partial discharges in gases with an admixture of CFN instead of SF_6 [9, 10, 12]. In [14], a 2D LFA fluid model was used to investigate the effect of buffer gases (either N_2 or CO_2) with admixtures of CFN, and the results were compared with results of similar SF_6 admixtures. It was shown that mixtures of N_2 with CFN have comparable insulation performance as mixtures of N_2 with SF_6. It showed that using CO_2 instead of N_2 as the buffer gas lowers the breakdown voltage. In [19], a 2D cylindrical LEA fluid model was used to study the effect of CFN fraction and voltage rise rate on negative streamers. The study showed that decreasing the voltage rise rate or increasing the CFN fraction led to higher breakdown voltages. Also shown is that fast voltage rise give normal negative streamers. Slow voltage rise results in stronger attachment, leading to less shielding of the streamer channel, and higher electric fields inside the channel. In our work we focused on negative streamers in CO_2 with admixtures of CFN using fully 3D models instead of 2D cylindrical models. We study how 3D fluid models perform compared to a 3D particle model.

1.3. Publications on 3D particle simulations with CFN admixtures

2D cylindrical fluid models, both with LFA or LEA, are computationally efficient, but they have important constraints:

(i) They are axisymmetric by construction. The models cannot simulate streamer branching or interaction of several streamers (except if they are aligned along one axis).
(ii) They are deterministic as the stochastic fluctuations of the particle models are averaged out.
(iii) In low-density regions a tiny fraction of a single electron can be present in a numerical grid cell, leading to numerical artefacts.

3D particle simulations as performed in [6] can overcome these shortcomings. In [6] negative streamers were simulated in CO_2 with admixtures of CFN in 3D using a particle-in-cell (PIC) Monte Carlo collision method. Different background fields and different mixtures of CFN and CO_2 were considered. The paper captured the stochastic behaviour of inception and branching, and found that fields close to breakdown are required for streamer propagation. It was also shown that the negative streamers will evolve as frequently branching streamer heads, with only a short conducting streamer channel.

1.4. The content of our paper: cross sections, Boltzmann solvers and 3D simulations

A downside of particle models is their high computational cost. In the present paper, we therefore investigate whether 3D fluid models can reproduce 3D PIC simulations of negative streamers in CO_2 with admixtures of CFN. High voltage insulation application use admixtures with typically not more than 10% CFN [20], hence we also used at must 10% CFN in the simulations

Another goal is to determine which cross section databases for electron-molecule interactions and which Boltzmann solver type should be used for the input data. PIC directly uses cross sections as input, while the fluid models require transport and reaction coefficients. These coefficients are calculated from the cross sections using Boltzmann solvers or a Monte-Carlo particle swarm code. We study the sensitivity of the coefficients on solver types at different mixture rates of CO_2 with CFN. We also test the different cross section datasets for CO_2 and CFN and determine the sensitivity of the reduced transport and reaction coefficients on these cross sections. The aim is to find a suitable solver and cross section dataset for the 3D fluid model. Then we test different LFA, LEA and PIC models in simulations of negative streamers.

1.5. Organisation of the paper

This work is structured as follows: in section 2, the transport and reaction coefficients are determined from the different available cross section databases. The sensitivity of these profiles to the input cross sections and to the used solver is probed, resulting in a recommendation for the cross section dataset and the Boltzmann solver to use. Next, in chapter 3, the fluid models and the particle model are explained in sections 3.1 and 3.2. The numerical setup and the initial and boundary conditions (B.C.s) are discussed in sections 3.3, 3.4, 5.2 and 5.3. The results of the fluid and the particle models are compared in sections 4.1–4.4. The discussion of this work is presented in section 5, and the conclusion is given in section 6.

2. Input data

2.1. Electron-neutral cross sections

We test cross section data sets derived by different authors, as collected on the LXCAT database [21–23]. For CFN, the databases of Flynn [24] and of Zhang [25] are tested. For CO_2, the databases of Hayashi [26, 27], Triniti [28], Phelps [29], Morgan [30], and IST-Lisbon [31, 32] are tested. The Phelps, Morgan, and IST-Lisbon cross sections for CO_2 include an 'effective' momentum scattering cross section, which we convert to an elastic cross section by subtracting the sum of all inelastic processes.

2.2. Comparing transport and reaction solvers

Fluid models require electron transport and reaction data, which can be computed from electron–neutral cross sections using a Boltzmann solver or a particle model. Since electrons attach very quickly to CFN in low fields, we were not sure whether the choice of solver type would affect the resulting transport data. We therefore tested two solvers: BOLSIG+ [33] and the `particle_swarm` code [34]. These solvers were used to calculate the reduced transport and reaction data for CO_2 with different admixture ratios of CFN. Reduced coefficients are studied as these are used in the fluid simulations as input. We used CO_2 with admixture of 1, 10, 20 or 50% CFN at 300 K and 1 bar so the gas number density is $N = 2.41 \times 10^{25}\,\mathrm{m}^{-3}$. Figure 1 shows the calculated reduced transport and reaction data, using the Flynn cross sections for CFN and the Hayashi cross sections for CO_2. We show the flux mobility and the flux transverse diffusion coefficient used in the fluid simulations.

From figure 1, we conclude that the two solvers produce similar coefficients for the reduced mobility μN, ionisation rate α/N, and attachment rate η/N. To quantify this, for each mixture and transport coefficient we have determined the average relative difference between the solvers. This was done by first computing relative differences and then taking the average of these relative differences. For α/N, the average was taken only for fields above 150 Td, to avoid division by zero. Average relative differences are below 3% for μN and α/N, and for η/N they are below 5%. The most significant deviations occur in low fields with a large fraction of CFN.

Significant deviations are observed for the transverse flux diffusion coefficient shown in figure 1. Transverse and bulk diffusion coefficients, which are not shown in the figure, also differ significantly between the solvers. The inaccuracy of the two-term approximation causes these discrepancies between solvers, see e.g. [35–38]. We have verified that a multiterm Boltzmann solver (Multibolt) with six terms [37] gives excellent agreement with the diffusion coefficients obtained with the `particle_swarm` code. Therefore we trust these two codes and use the `particle_swarm` code to calculate the input coefficients for the fluid simulations.

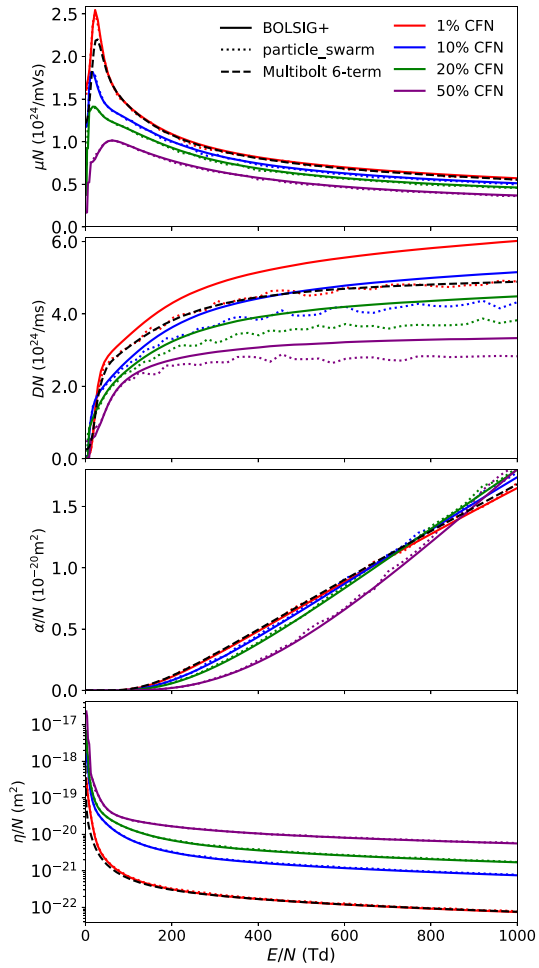

Figure 1. Comparison of the reduced flux transport and reaction coefficients calculated with BOLSIG+ (solid lines) and `particle_swarm` code (dotted lines). The coefficients are flux coefficients and were calculated for CO_2 with admixtures of $1\%, 10\%, 20\%$ and 50% CFN as a function of E/N. Cross section data of Hayashi for CO_2 and Flynn for CFN were used. μN, α/N, and η/N agree well, while DN differs as discussed in the main text. Multibolt results of CO_2 with 1% CFN using 6-terms is added as the dashed line to show that `particle_swarm` DN does agree with higher-order Boltzmann solvers.

2.3. Dependence on cross sections

We now determine how the choice of cross sections affects reduced transport and reaction data in pure CFN, using BOLSIG+ with $N = 2.41 \times 10^{22}\,\mathrm{m}^{-3}$ at 300 K and 1 mbar. Experimental CFN swarm data are only available at $\leqslant$1 mbar, therefore we also calculated the coefficients at 1 mbar in the comparisons with experiments. This in contrasted to the calculations in section 2.2 and the 3D simulations, where 1 bar is used. For this comparison, we computed the bulk mobility, the bulk longitudinal diffusion coefficient and the effective ionisation rate defined as $k_{\mathrm{eff}} = k_\alpha - k_\eta$. Here is $k_\alpha = \alpha v_{\mathrm{drift}}$ and $k_\eta = \eta v_{\mathrm{drift}}$ with v_{drift} the electron drift velocity. Swarm experiments provide bulk coefficients and k_{eff}, so we also calculate these in this section. Note that α, η and flux coefficients for μ and D are used as input for the simulations. Figure 2 shows results in pure CFN, using either the Zhang or the Flynn cross sections. There are clearly significant differences in $k_{\mathrm{eff}}/N, \mu N$ and DN, for which we have no explanation. Experimental swarm data for pure CFN are only available between 700 Td and 1050 Td [39, 40], and are plotted as black points in figure 2. Hence, it is difficult to conclude which CFN cross section set is to be preferred. Note the solver did not converge at small E/N, leading to numerical artefacts shown in figure 2.

However, in CO_2 with admixtures of CFN, swarm data have been measured over a wide range of reduced electric fields [40, 41] and these data are available on LXCat [23]. In figure 3, reduced coefficients calculated from different CFN and CO_2 cross section datasets are compared with experimental swarm data, for 1% and 10% CFN at 100 Pa and 296 K. For this comparison, we computed the bulk mobility, the bulk longitudinal diffusion coefficient and k_{eff}/N using the `particle_swarm` code.

In contrast to the case of pure CFN, the CFN cross sections of either Zhang or Flynn now result in similar transport data for the considered CFN admixtures in CO_2. The only exception is that k_{eff}/N becomes significantly more negative with the Zhang cross sections for small E/N with 10% CFN. The

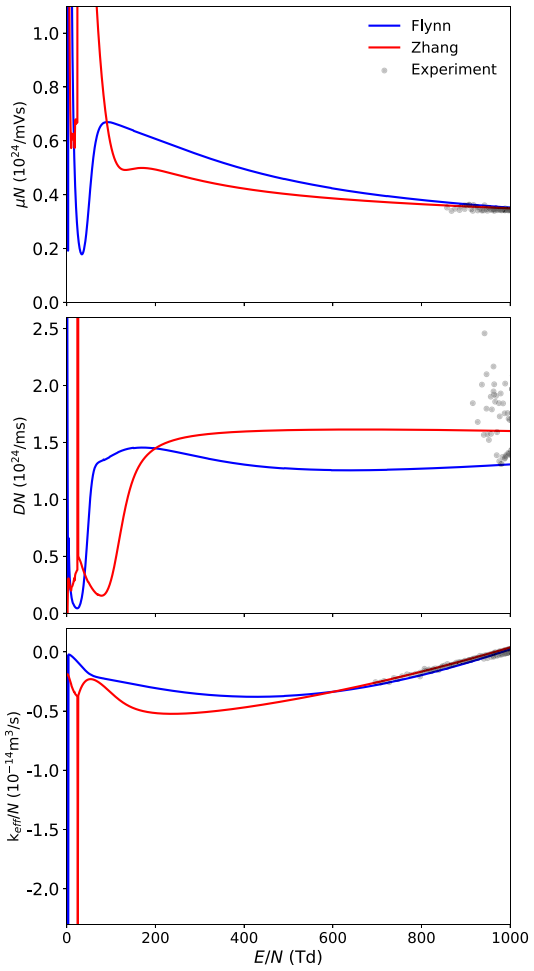

Figure 2. Comparison of the Flynn and Zhang reduced transport and reaction coefficients in pure CFN as functions of E/N. The coefficients are flux coefficients and were calculated with BOLSIG+. Differences of up to 40% for all coefficients are observed. The black points indicate experimental swarm data from [39, 40]. BOLSIG+ did not converge at small E/N, leading to numerical artefacts.

coefficients in pure CO_2 are given in the appendix for comparison. Due to the small effect of the different CFN cross sections, only one set of coefficients based on the Zhang cross section is shown in figure 3. Since the mixtures predominantly contain CO_2, the transport data are more sensitive to the choice of CO_2 cross sections. For $\mu_{\text{bulk}}N$, there is good agreement between the experimental data (black points) and data computed using the Triniti and Hayashi databases. For k_{eff}/N, good agreement is only obtained with the Hayashi database. The agreement between the calculated and the experimental diffusion data is generally worse, in particular for fields above 600 Td. The best agreement between calculated and experimental diffusion data is obtained with the Morgan database, closely followed by the Hayashi database.

Since the electron mobility and the effective ionisation coefficient are the most important input data in a fluid model, we will use the Hayashi CO_2 cross sections in our simulations. The panels in figure 3 do not show significant differences when using either the Zhang or the Flynn cross sections for CFN, so we have made the rather arbitrary choice to use the Flynn cross sections. The critical fields E_k for CO_2 with CFN admixtures using Hayashi and Flynn cross sections are given in table 1.

The attachment and ionisation processes included in these databases are listed in table 2. Other elastic and inelastic collisions are included in the cross-section data of CO_2 and CFN and are therefore also included in the calculation of the transport and reaction coefficients. To reduce the computational cost, only the species e^-, CO_2^+, O^-, $C_4F_7N^-$, C_4F_7N and CO_2 from table 2 are tracked. All other species are collected into either M^-, M^+ or M based on their charge. This does not alter the model's predictions, as no detachment or recombination reactions are considered. $M^\pm$ are included in ρ for the Poisson calculation. We assume that all atoms, molecules and ions are immobile.

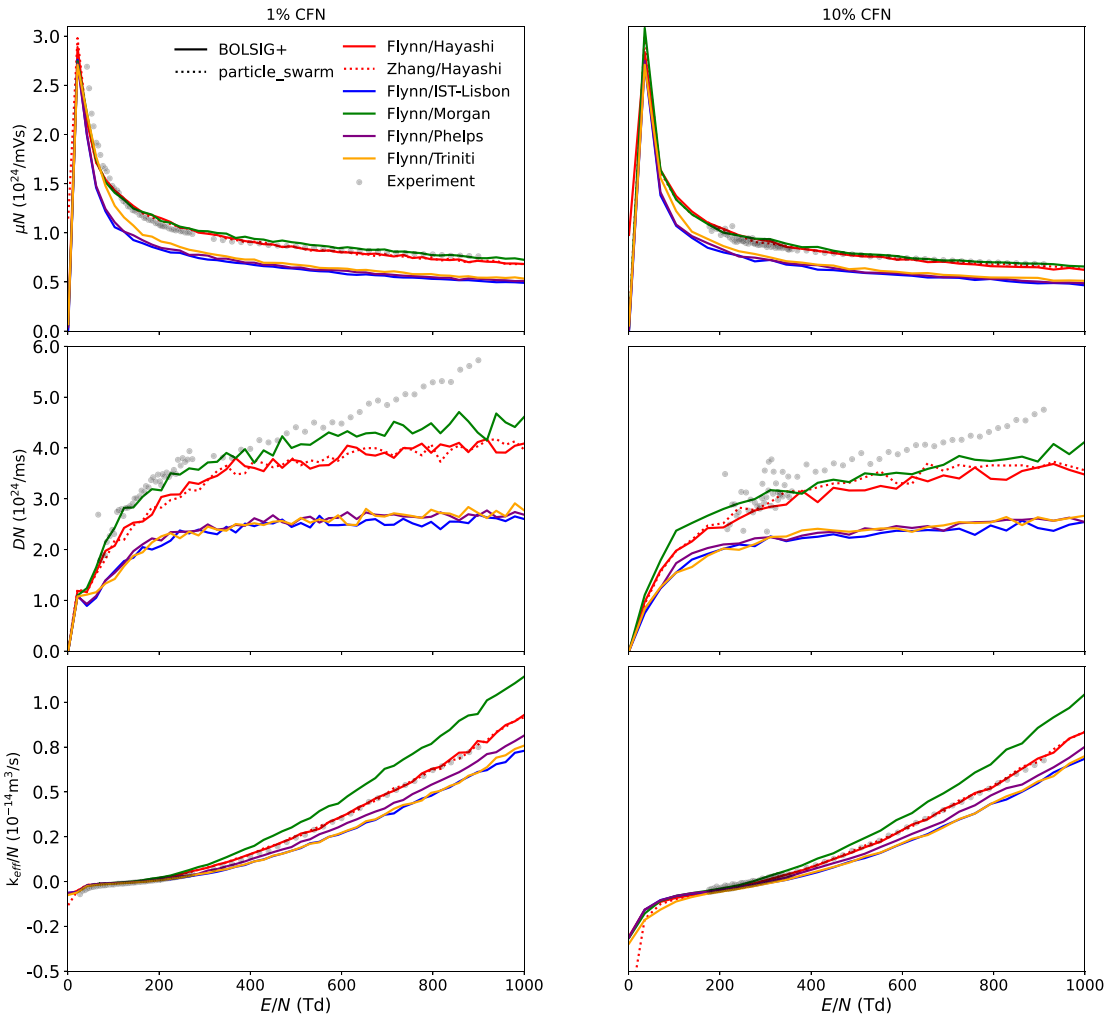

Figure 3. Comparison of reduced transport and reaction coefficients of different CO_2 databases with an admixture of 1% (left) or 10% (right) CFN as functions of E/N. The coefficients are bulk coefficients, and were calculated with the `particle_swarm` code. The black points indicate experimental swarm data from [40, 41] at 296 K and 1 mbar. The CFN cross sections here have a minor influence, so for the Zhang database only the combination with the Hayashi CO_2 cross section is shown. The Flynn cross sections are used to calculate the input data for the fluid simulations. Experimental data agree well with the Flynn/Hayashi and Zhang/Hayashi results.

Table 1. Critical electric field E_k for CO_2 with different admixtures of CFN with $N = 2.41 \times 10^{25}\,\mathrm{m}^{-3}$ at 300 K and 0.1 MPa. Hayashi cross sections for CO_2 and Flynn cross sections for CFN are used. The critical field E_k is defined as the field where the ionisation rate α equals the attachment rate η.

Admixture of CFN	E_k
pure CO_2	$18.0\,\mathrm{kVcm}^{-1}$
1% CFN	$35.4\,\mathrm{kVcm}^{-1}$
10% CFN	$69.3\,\mathrm{kVcm}^{-1}$
20% CFN	$96.5\,\mathrm{kVcm}^{-1}$
50% CFN	$157.3\,\mathrm{kVcm}^{-1}$
100% CFN	$234.7\,\mathrm{kVcm}^{-1}$

3. Simulation models

3.1. Fluid models: LFA and LEA

In this work, two types of reaction-drift-diffusion fluid models for electrons are considered [17, 18]: the LFA and the LEA. The LFA model is commonly used, but it may fail to capture non-local effects [42, 43]. The classical LFA model is given by

Table 2. The attachment and ionisation reactions included in the simulations. CFN reactions are from Flynn [24], and CO_2 reactions are from Hayashi [26, 27]. For the complete reaction list of CFN see [24] and of CO_2 see [26, 27].

Ionization
$e + CO_2 \rightarrow e + e + CO_2^+$
$e + C_4F_7N \rightarrow e + e + C_3F_4N + CF_3^+$
$e + C_4F_7N \rightarrow e + e + CF_4 + C_3F_3N^+$
$e + C_4F_7N \rightarrow e + e + F + C_4F_6N^+$
$e + C_4F_7N \rightarrow e + e + C_2F_5 + C_2F_2N^+$
$e + C_4F_7N \rightarrow e + e + C_3F_4N + F_2 + CF^+$
$e + C_4F_7N \rightarrow e + e + C_2F_3N + C_2F_4^+$
$e + C_4F_7N \rightarrow e + e + C_3F_5N + CF_2^+$
$e + C_4F_7N \rightarrow e + e + C_2F_6 + C_2FN^+$
Attachment
$e + CO_2 \rightarrow CO + O^-$
$e + C_4F_7N \rightarrow C_4F_7N^-$
$e + C_4F_7N \rightarrow F + C_4F_6N^-$
$e + C_4F_7N \rightarrow CF_3 + C_3F_4N^-$
$e + C_4F_7N \rightarrow C_4F_6N + F^-$
$e + C_4F_7N \rightarrow C_3F_7 + CN^-$
$e + C_4F_7N \rightarrow C_4F_6N + F^-$
$e + C_4F_7N \rightarrow F + C_4F_6N^-$

$$\partial_t n_e + \nabla \cdot \Gamma_e = S_e, \tag{1}$$
$$\partial_t n_{ion} = S_e, \tag{2}$$
$$\Gamma_e = -\mu_e(E)\mathbf{E}n_e - D_e(E)\nabla n_e, \tag{3}$$
$$S_e = n_e \mu_e(E) E \alpha_{eff}(E). \tag{4}$$

Here, n_e is the electron density, n_{ion} is the density of positive minus negative ions, $\mathbf{E}$ is the electric field and $E = |\mathbf{E}|$ its magnitude, S_e is the source term due to ionisation and attachment, Γ_e is the electron flux and α_{eff} the effective ionisation coefficient defined as $\alpha_{eff} = \alpha - \eta$.

The LEA model used here is given by:

$$\partial_t n_e + \nabla \cdot \Gamma_e = S_e, \tag{5}$$
$$\partial_t n_{ion} = S_e, \tag{6}$$
$$\partial_t(n_e\epsilon) + \nabla \cdot \Gamma_\epsilon = S_\epsilon, \tag{7}$$
$$\Gamma_e = -\mu_e(\epsilon)\mathbf{E}n_e - D_e(\epsilon)\nabla n_e, \tag{8}$$
$$\Gamma_\epsilon = -\frac{5}{3}\left[\mu_e(\epsilon)\mathbf{E}n_e\epsilon + D_e(\epsilon)\nabla(n_e\epsilon)\right], \tag{9}$$
$$S_e = n_e \mu_e(\epsilon) E \alpha_{eff}(\epsilon), \tag{10}$$
$$S_\epsilon = -\mathbf{E} \cdot \Gamma_e - P_{loss}. \tag{11}$$

Here ϵ is the local average electron energy, $(n_e\epsilon)$ is the electron energy density, $\mathbf{\Gamma}_\epsilon$ is the energy flux, S_ϵ is the energy source term. P_{loss} is the electron energy loss rate due to (in)elastic collisions

$$P_{loss} = \mu_e(\epsilon) E(\epsilon)^2, \tag{12}$$

where $E(\epsilon)$ is the electric field strength corresponding to the mean energy ϵ in the input data. This expression is based on the observation that for an electron swarm the average energy gain should equal the average energy loss, see e.g. page 19 of the documentation of BOLSIG+ [33]. Both `particle_swarm` and BOLSIG+ calculate the transport and rate coefficients and ϵ as a function of E/N. The $\epsilon(E/N)$ data allows us to remap the coefficients as a function of ϵ.

The fluid models are coupled with the electric field, computed in the electrostatic approximation as

$$\nabla^2\phi = -\frac{\rho}{\epsilon_0} \tag{13}$$
$$\mathbf{E} = -\nabla\phi, \tag{14}$$

where $\rho = e(n_{\text{ion}} - n_e)$ is the charge density, ϵ_0 is the vacuum permittivity, and ϕ is the electric potential. For both models, the afivo-streamer code [44, 45] is used. Afivo-streamer is a fluid-model for streamer simulations, using a finite-volume method. It is based on the Afivo framework [44], which provides adaptive mesh refinement and a geometric multigrid solver for Poisson's equation. This paper presents the first use of the LEA model within the afivo-streamer code.

With the LFA model, unphysical effects due to electron diffusion against the electron drift direction can occur [46, 47]. This can cause electrons to diffuse into the sheath near a negative electrode, where the field and therefore α_{eff} are high, resulting in a rapid growth of the electron density. Therefore, a correction factor for the LFA electron source term is used

$$f_e = \max\left(0, 1 - \frac{\hat{\mathbf{E}} \cdot \Gamma_{\text{diffusion}}}{\|\Gamma_{\text{drift}}\|}\right), \tag{15}$$

where Γ_{drift} and $\Gamma_{\text{diffusion}}$ are the drift and diffusive components of the electron flux and $\hat{\mathbf{E}}$ is the electric field unit vector, see [46, 47] for details. This factor can be derived from the energy conservation in equation (7) as is shown in [46]. Unphysical ionisation is not fully avoided with f_e, but delayed, as discussed in section 5.2.

3.2. Particle model

We use a PIC Monte Carlo collision model as implemented in the afivo-pic code [48], and also used in `particle_swarm`. Electrons are tracked as particles, and ions as immobile densities. The electron velocity and position are updated with the velocity Verlet scheme. The gas is modelled as a background that electrons stochastically collide with using the null-collision method [49, 50]. The input for the PIC model are the electron–neutral cross sections. We use the same scattering algorithm and electron–neutral cross sections in both `particle_swarm` and PIC model. We assume isotropic scattering for consistency with the cross sections used For computational efficiency, electrons are grouped into super-particles with adaptive weights. The weights are changed so that the number of particles per cell roughly stays below 100, see [48] for more details.

3.3. Computational domain and grid refinement

We use a 5 mm × 5 mm × 10 mm computational domain with a plate-to-plate geometry and a protruding rod electrode at the top, see figure 4; the same configuration was also used in [6]. The rod electrode is 2 mm long and has a semi-spherical tip with a diameter of 0.4 mm. This relatively narrow and short domain reduces the computational cost of the simulations, but we also provide simulations in a larger computational domain in section 4.4. Adaptive time stepping is used, with the time step limited by the most restrictive timescale, see [45].

We evaluate the models at $N = 2.41 \times 10^{25}\ \text{m}^{-3}$ with varying admixtures of CFN. The simulations use the adaptive mesh refinement of the Afivo model [44]. The refinement condition is $\alpha_{\text{eff}}\Delta x \leqslant 1.0$ with α_{eff} the effective ionization constant. This criterion is usually sufficient to obtain well-converged PIC and fluid simulations of streamers [51]. The resulting minimal grid spacing is about 2.4 μm for the simulations presented here. The maximum grid spacing in the simulations is limited to $\Delta x \leqslant 55\,\mu$m. We remark that numerical heating can occur in PIC simulations when the Debye length is not resolved, but as discussed in B this effect is not significant here, mainly because we consider a weakly ionized plasma.

3.4. Initial and B.C.s

At the planar bottom boundary, we set $\phi = 0$, and at the top boundary, including the protruding electrode, $\phi = V_0$, where V_0 is the applied (negative) voltage. We use the same definition of the background field as in [6], so that $E_{\text{bg}} = |V_0|/d_{\text{plate}}$ with $d_{\text{plate}} = 10$ mm. Neumann zero B.C.s ($\hat{\mathbf{n}} \cdot \nabla\phi = 0$, where $\hat{\mathbf{n}}$ is an unit vector perpendicular to the boundary) are applied on the sides of the domain. For the ion and electron densities, a Dirichlet zero boundary condition ($n_e = 0$) is used on all domain boundaries including the electrodes. The effect of Neumann and Dirichlet conditions on the species is discussed in section 5.3.

As an initial condition, we place 15 single electrons (i.e. with super-particle weight of 1) near the electrode. Their initial locations are sampled from a Gaussian distribution centred 0.2 mm below the electrode tip with a width of 0.2 mm, and we place electron-CO_2^+ pairs at these locations. While the PIC model operates with electrons as particles, in the fluid models these 15 electrons at the start of the simulation are converted to densities by dividing the number of electrons per cell by the volume of the cell. For better comparison between the models the same 15 initial positions are used in all simulations performed with the particle and fluid models; they are shown in figure 4.

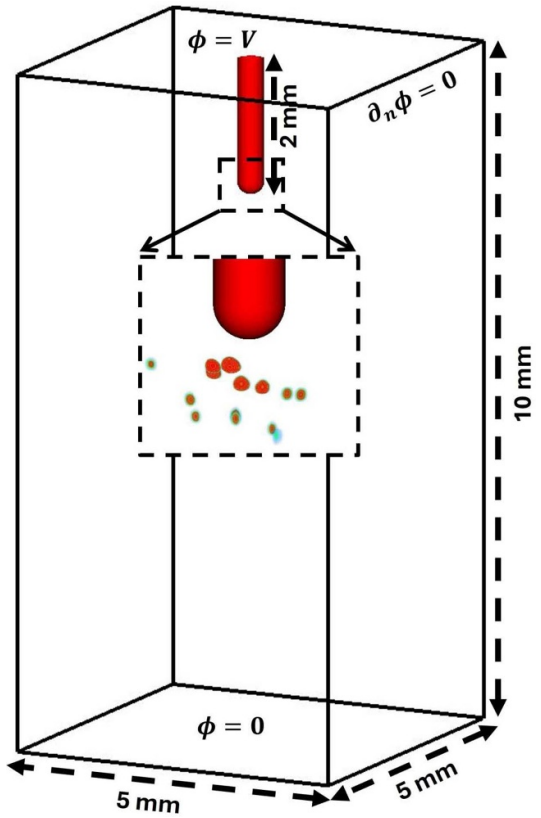

Figure 4. A view of the plate-to-plate computational domain of 5 mm × 5 mm × 10 mm with protruding top electrode of 2 mm. The dashed box zooms into the location of the stochastic initial condition after the first time step of 0.2 ns.

4. Fluid versus particle models

4.1. Comparison of the three models at 36.1 kV cm^{-1}

We first present simulations in CO_2 with an admixture of 1% CFN in a background field of 36.1 kVcm^{-1} which is slightly above $E_k = 35.4$ kV cm^{-1} (see table 1). For these parameters we compare the simulation results of the LFA, LEA and particle models and show them in figures 5–7.

Initially, the streamer morphologies and densities are highly similar, as shown in figures 5 and 7(a). After about 6 ns, the main difference is that there is branching in the particle model, as expected. The particle model is stochastic in nature as particles scatter according to a Monte Carlo procedure, and stochastic density fluctuations are artificially enhanced due to the use of super-particles (see section 3.2). Such dynamic density fluctuations are absent in the deterministic fluid models.

The charge density ρ at time $t = 8$ ns is shown in figure 6(a). The PIC simulations show a rather noisy charge density created by the many small streamer branches, whereas the charge density in the fluid simulations is much smoother. The models start with a stochastic initial condition, which largely fades out in the fluid models. The particle model remains stochastic, as it simulates the random motion of particles. The stochastic effects will be discussed in more detail in section 5.4

The electric field magnitude over planes perpendicular to the streamer is shown in figure 6(b). In all models we observe 'isolated' streamer heads, which only have a short conductive channel where the electric field is screened. Further back, the field relaxes to the background field, which happens more smoothly in the fluid simulations.

The peak field is obtained by taking the maximum value of the electric field magnitude across the transverse directions as a function of the z-coordinate. Figure 7(b) shows the peak field values. In the PIC and LFA models, the peak electric field stays around 120 kVcm^{-1} in the whole gap, whereas this value increases to about 140 kVcm^{-1} in the LEA model when the streamer has almost bridged the gap. Overall, the behaviour between the models is qualitatively similar, with deviations not exceeding ∼15% for the peak field in figure 7(b) or ∼30% for max(n_e) in figure 7(a). In all cases, a main peak due to the fastest streamer is followed by smaller peaks corresponding to slower streamers.

From figure 7(a), we have determined the velocities of the fastest streamer between $z \approx 7$ mm and $z \approx 1$ mm: $v_{\mathrm{LEA}} \approx 0.70$ mm ns^{-1}, $v_{\mathrm{LFA}} \approx 0.56$ mm ns^{-1}, and $v_{\mathrm{PIC}} \approx 0.60$ mm ns^{-1}. The LEA streamers are

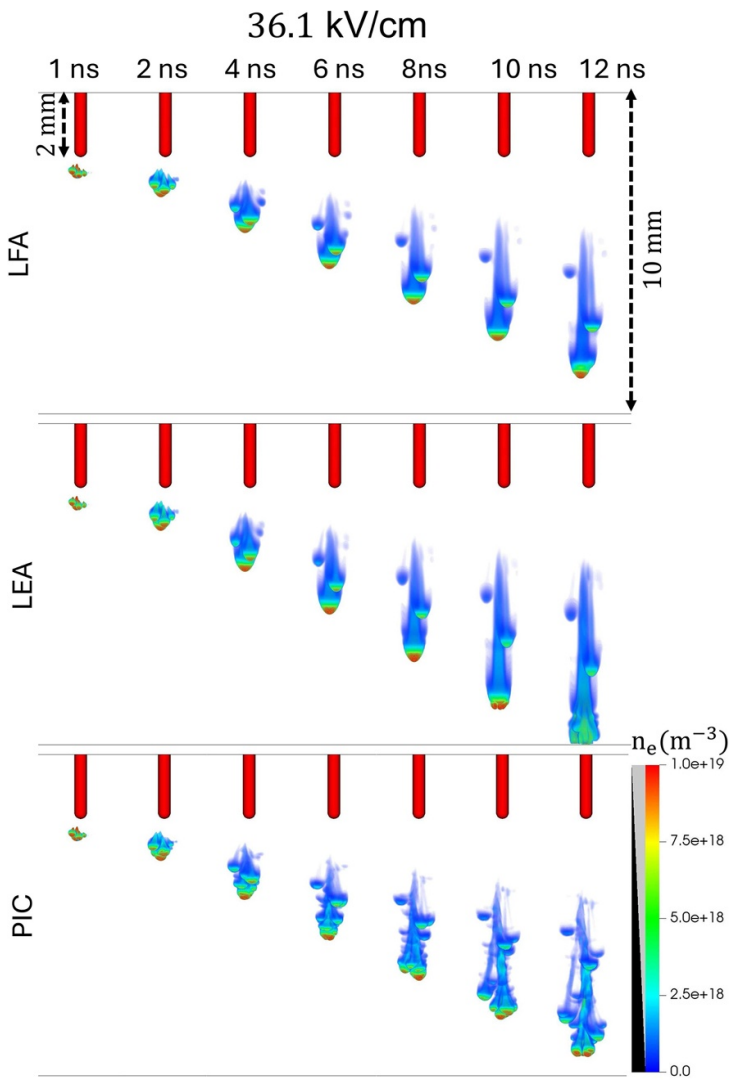

Figure 5. Evolution of the electron density of the LFA, LEA and PIC models for CO_2 with an admixture of 1% CFN in a background field of $E_{bg} = 36.1\,\mathrm{kVcm}^{-1}$. The simulations show the same initial stochastic growth, with some disagreement in later phases due to branching. Figures are generated using ray-traced 3D volume rendering in Visit [52].

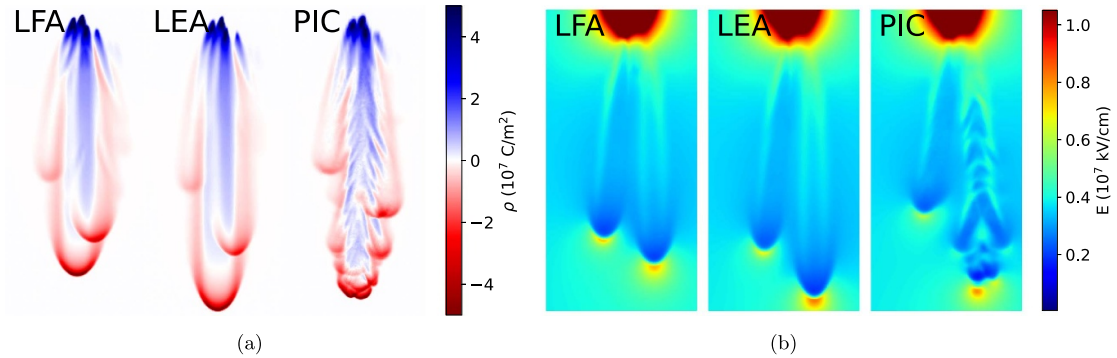

(a) (b)

Figure 6. (a) The charge density ρ integrated along the line of sight on the xz-plane at time 8 ns. Shown are the simulation data of figure 5. Red indicates negative and blue positive charge densities. The profiles are similar, with the main difference that there is more branching in the particle model. (b) Electric field magnitude in the yz-plane, where z is the direction of the background field at 8 ns, showing again the simulation data from figure 5. The saturated red region indicates the high field near the electrode. The E are similar in the streamer heads for the three models. The major difference is again the branching.

thus the fastest, while the LFA and PIC results agree rather well. The higher velocity of the LEA streamers is related to their slightly higher maximal electric field and therefore higher electron drift velocity (as negative streamers should propagate at least with the drift velocity); see figure 7.

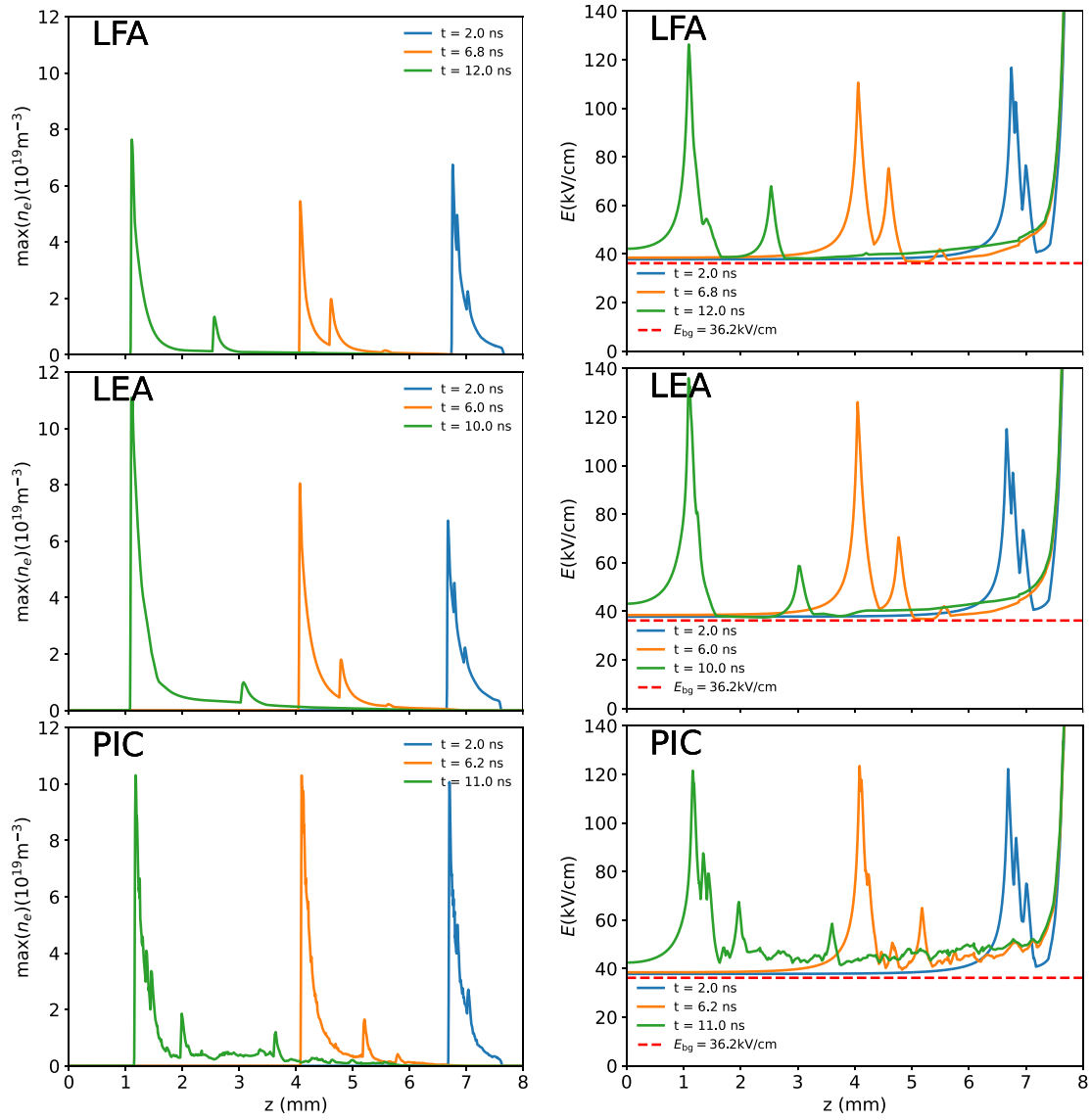

(a) Maximum electron density (b) Maximum electric field magnitude

Figure 7. Comparison of (a) maximum electron density and (b) maximum electric field magnitude over the transverse directions as a function of the z-coordinate of the LFA, LEA, and PIC simulations in figure 5. Three instances (marked by different colors) are chosen where the fastest streamers have roughly the same length. The z-axis is truncated at $z = 8$ mm to exclude the electrode. The models produce comparable profiles, with PIC showing a noisier distribution.

The deviations in velocity between the LEA and PIC are somewhat puzzling. We expected LEA and PIC to be similar as both account for the higher electron energies that the electrons gain while propagating at v_{drift}, as shown in [42]. However, the PIC streamer branches, causing partial screening of the streamer heads. This reduces the field enhancement and maximum field to be more similar to the LFA model. Since a negative streamer propagates at least with v_{drift} at the maximum field, this branching also reduces the PIC velocity toward the LFA velocity.

Another cause of the deviations can be the prefactor 5/3 in equation (9) which is based on [17, 18]. It is an approximation and can deviate for different gas mixtures. The correct prefactor can be obtained from BOLSIG+/`particle_swarm`, but we choose to use this simple LEA model to show the practicality of fluid models. Alternative LEA formulations exist [53]. In conclusion, the exact cause of the velocity difference is difficult to pinpoint precisely in this 3D non-linear model.

4.2. Comparison of model results in different fields

Figure 8 shows simulation results in CO_2 with an admixture of 1% CFN, but now at background fields of $E_{\text{bg}} = 32.0$, 34.2 and 38.2 kVcm^{-1}, which are near $E_k = 35.4$ kVcm^{-1}. With a higher background field

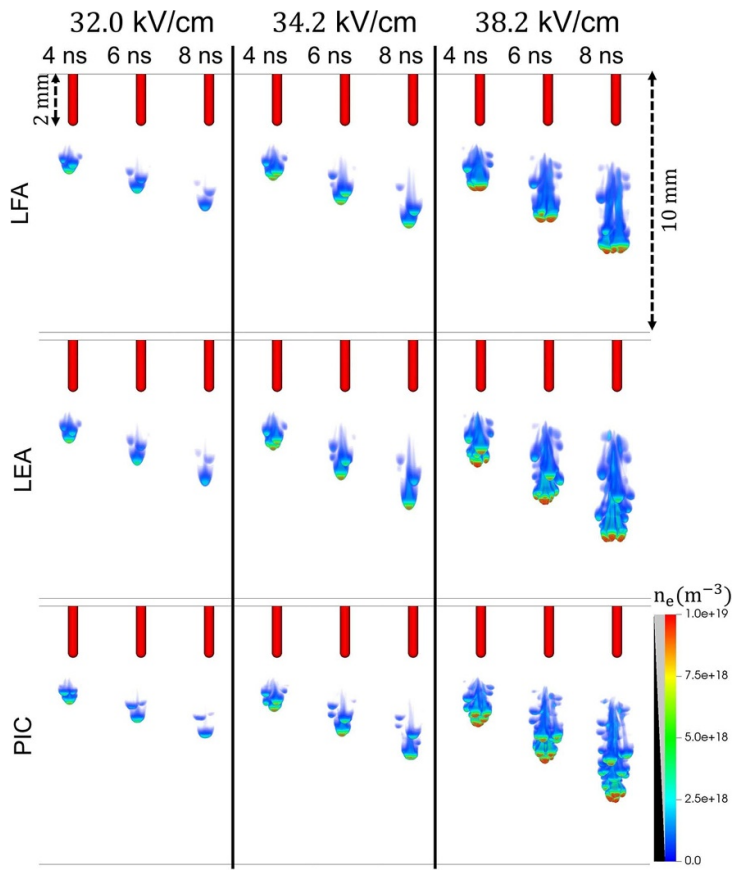

Figure 8. Evolution of the electron density with the same parameters as in figure 5 except for the background field being here $E_{bg} = 32.0\,\mathrm{kVcm^{-1}}$, $34.2\,\mathrm{kVcm^{-1}}$ and $38.2\,\mathrm{kVcm^{-1}}$ with from left to right; in figure 5 it was 36.1 kV/cm. Three time steps for simulations with the three models are shown. At low E_{bg}, the evolution is similar. At higher E_{bg}, more branching occurs making the fluid and particle models less similar.

the streamers have a longer conductive channel and there is significantly more streamer branching. The particle simulations still branch more often, which is again the most prominent difference between fluid and particle simulations. Similar to the case at $36.1\,\mathrm{kV\,cm^{-1}}$, streamers are the slowest with the LFA model and the fastest with the LEA model, with differences of 10%–20%.

4.3. Model comparison with 10% CFN

Next, we consider an admixture of 10% CFN at $63\,\mathrm{kVcm^{-1}}$ which is below E_k, see table 1. The results of the LFA, LEA and particle models are shown in figure 9. With all models, we observe streamer heads with a short conductive channel that fade out after propagating approximately halfway through the gap. The LEA streamers are again the fastest, with the LFA and PIC velocities agreeing well, similar to the cases with a lower CFN fraction.

4.4. Larger computational domain

The simulations presented above were performed in a relatively small computational domain of $5\,\mathrm{mm} \times 5\,\mathrm{mm} \times 10\,\mathrm{mm}$. We have also simulated streamers in a larger domain of $10\,\mathrm{mm} \times 10\,\mathrm{mm} \times 20\,\mathrm{mm}$ while keeping the same needle size to reduce the effect of the lateral B.C.s. The simulations were performed with an admixture of 1% CFN at $E_{bg} = 34.2\,\mathrm{kVcm^{-1}}$ and $36.1\,\mathrm{kVcm^{-1}}$. Results of the LFA, LEA and particle models are shown in figure 10.

At $34.2\,\mathrm{kVcm^{-1}}$ all models produce isolated streamer heads with only a short channel. These streamers stop propagating at about 5 mm below the electrode. Within the smaller domain the streamer crossed the gap at this background field, see figure 8. However, it should be noted that we define the background field as the average field between the plates. When the background fields are equal, the *average* field between the electrode tip and the opposite plate will be lower in the larger computational domain.

At $E_{bg} = 36.1\,\mathrm{kVcm^{-1}}$ the streamers have much longer conductive channels. Therefore the voltage drop over the length of the channel decreases and a larger voltage drop is available at the streamer head,

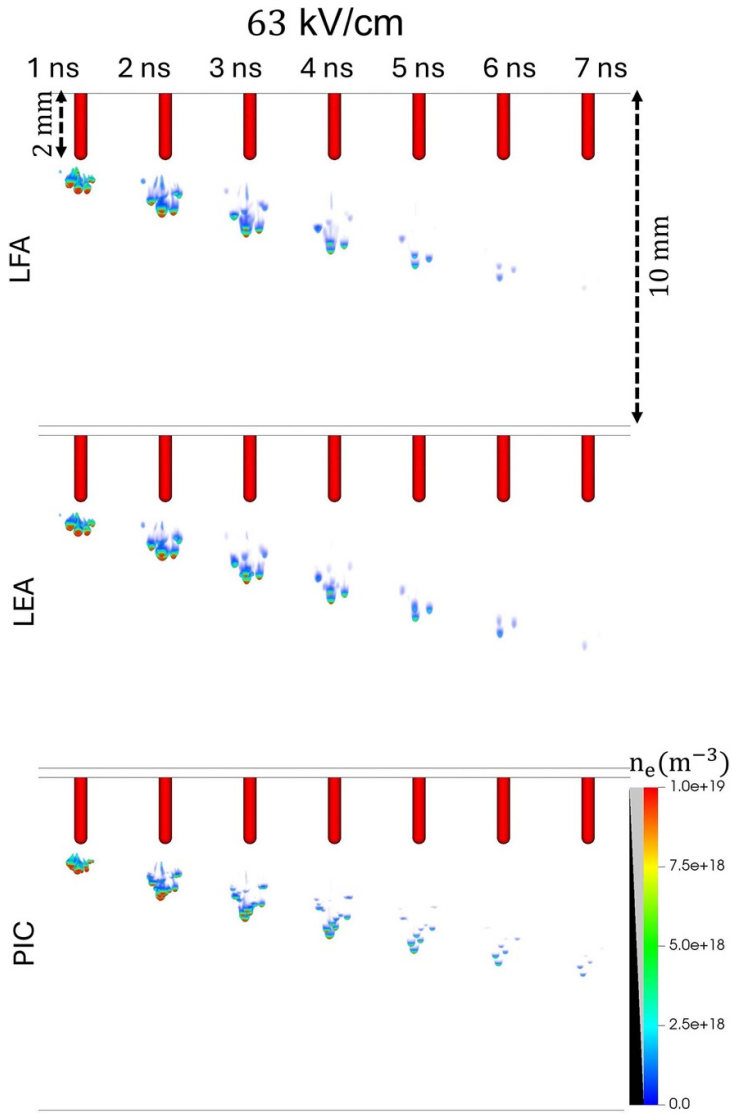

Figure 9. Evolution of the electron density, now in CO_2 with an admixture of 10% CFN. The background field now is $E_{bg} = 63\,\mathrm{kVcm^{-1}}$, slightly lower than the critical field $E_k = 69.3\,\mathrm{kV\,cm^{-1}}$. The models show similar initial growth across the different models, with some disagreement in the later phase of the simulation. All models predict streamers to fade.

creating a larger electric field at that location. This is particularly the case for the LEA model, which again produces the fastest streamers, whereas the PIC and LFA velocities agree quite well.

5. Discussion

5.1. Computational cost

The simulations were performed on 'Rome' computing nodes of the Snellius supercomputer (SURF, the Netherlands), which have dual AMD EPYC 7H12 CPUs with a total of 128 cores. For each simulation a quarter (32 cores) of a single node was used. The approximate run times of the simulations in 4.1 and 4.2 are summarised in table 3.

The particle model only refined grid cells in which $n_e \geqslant 10^{13}\,\mathrm{m^{-3}}$, so it generally used fewer grid cells than the fluid models. At low E_{bg}, the use of relatively few super-particles (around 10^7) resulted in PIC having the shortest run times. At higher E_{bg}, the number of super-particles increased (up to 10^8), which slowed down PIC, and the LFA became faster. The LEA model was always the slowest, which was caused by two main factors: a finer grid due to the slightly higher electric field at streamer tips, and a smaller time step due to the extra energy equation. The specific initial conditions used (e.g. few seed particles and strong attachment) makes that PIC is only ∼2 times slower, as we only have a small volume containing particles.

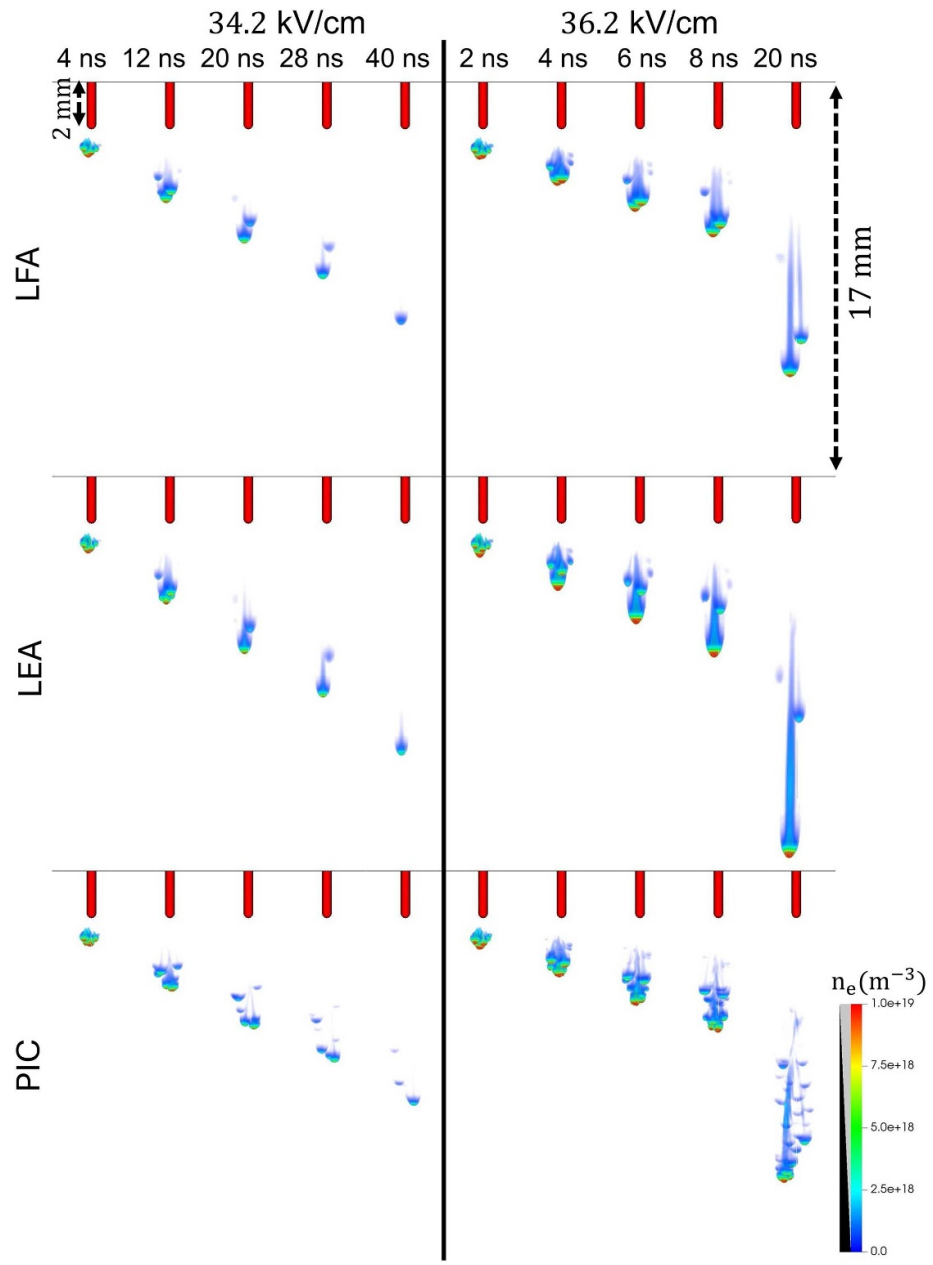

Figure 10. Evolution of the electron density within the larger domain in CO_2 with an admixture of 1% CFN in a background field of $E_{bg} = 34.2\,\mathrm{kVcm^{-1}}$ (left) and $36.1\,\mathrm{kVcm^{-1}}$ (right). The figure only shows the top 17 mm, to exclude empty space between the steamer and bottom electrode. Again, similar streamers are produced with the different models.

5.2. Sensitivity to initial conditions

As is shown in section 3.1 and in [54], the LFA model can have issues resolving the cathode sheath. The sheath issue is illustrated in figure 11, which shows LEA and LFA simulations in which the initial electrons were shifted 0.1 mm towards the electrode tip in comparison to the simulations shown earlier in section 4.1.

With the LFA model, the back side of a negative streamer grows towards the needle, resulting in a small region with an electron density as high as about $10^{22}\,\mathrm{m^{-3}}$. This high density keeps increasing, and due to the resulting small dielectric relaxation time $\Delta t < \epsilon_0/(e\mu_e n_e)$ [45] the simulation effectively stops. Such unphysical growth is not present in the LEA model under the conditions and time scale considered here.

Note that in our LFA simulations, we have used a correction factor for the source term, as shown in equation (15). This factor reduces the unphysical growth, but does not completely stop it, as is evident in figure 11. In general, one should therefore avoid initial conditions that lead to a cathode sheath when using the LFA model.

Table 3. The approximate simulation times of the runs in sections 4.1 and 4.2.

E_{bg}	LFA	LEA	PIC
32.0 kV cm^{-1}	∼ 19 h	∼ 65 h	∼ 5 h
34.2 kV cm^{-1}	∼ 36 h	∼ 64 h	∼ 18 h
36.1 kV cm^{-1}	∼ 25 h	∼ 84 h	∼ 44 h
38.2 kV cm^{-1}	∼ 34 h	∼ 108 h	∼ 79 h

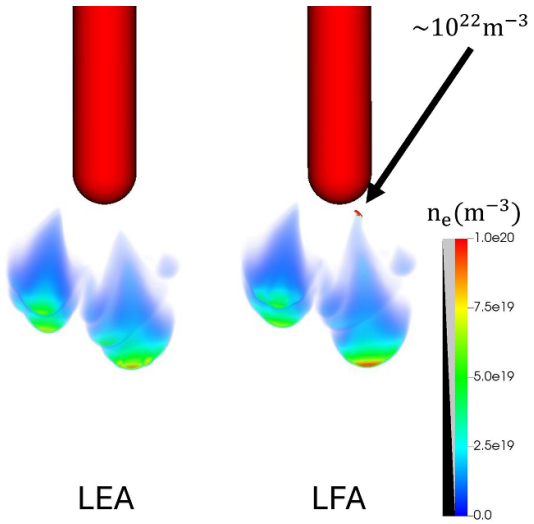

Figure 11. A close-up of the electron density near the electrode with the seed placed closer to the electrode. In LFA a tail moving backwards towards the electrode appears, which does not appear in LEA for the considered parameters. The density in this tail quickly increases due to fast ionisation, effectively stopping the LFA simulation, as the required time step keeps decreasing.

5.3. Neumann versus Dirichlet B.C.s

Commonly a Neumann zero boundary condition ($\hat{\mathbf{n}} \cdot \nabla n_e = 0$) is used for n_e on the electrode for positive streamers. In this case, electrons flow into the electrode from which the streamers are emitted. However, for negative streamers electrons can flow out of the electrode, making the B.C.s more important. We therefore study the effect of Dirichlet or Neumann B.C.s for the electron density at the electrode. We use CO_2 with an admixture of 1% CFN in a background field of 36.1 kVcm^{-1} in the LFA model.

A close-up of the electron dynamics near the electrode is shown in figure 12. In the first two stages of figure 12 the number of initial avalanches and their morphology and electron densities are rather indistinguishable between the two B.C.s. The difference emerges after 0.6 ns as in the case of the Neumann B.C., structures with a high electron density form near the electrode. These high densities result in a short dielectric relaxation time, which limits the global time step. These high electron density structures form after a small electron density has diffused towards the electrode. Most of these electrons drift away, causing the flux at the electrode to be non-zero. This results in an outflow of electrons with Neumann zero B.C.. The combination of this outflow with the local high electric field causes ionisation, resulting in rapidly growing n_e effectively stopping the simulation. This outflow is absent with a Dirichlet B.C., preventing high n_e formation in the initial phase. Dirichlet zero B.C. approximates a scenario where electrons do not have sufficient energy to overcome the electrode work function, such that there is no electron emission. The short timescales of 20 ns considered in this work result in a small ion flux and low secondary electron emission, thus Dirichlet B.C. are more suitable.

5.4. Stochastic effects

The initial condition for the electrons is stochastic, as described in section 3.4. The dynamic evolution of the fluid models is deterministic, while the particle model is stochastic. Thus, it is understandable that the particle model branches more frequently than fluid models, as shown in section 4. Branching can occur due to physical density fluctuations. The particle model overestimates density fluctuations due to the use of super-particles, where the fluctuations are increased by a factor of $\sqrt{w}$, with w the particle

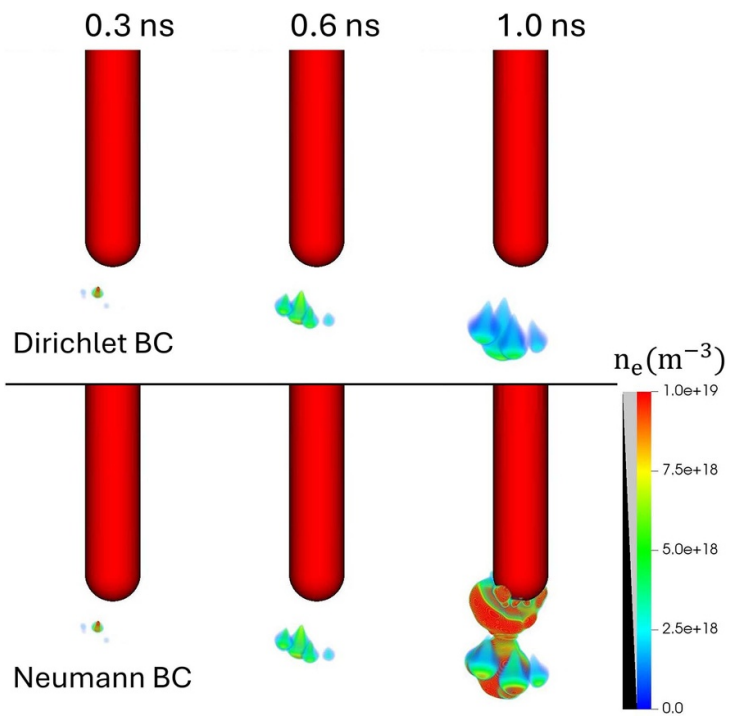

Figure 12. The evolution of the electron density near an electrode with either Dirichlet (top) or Neumann (bottom) zero boundary conditions using the same parameters as in 4.2 s.t. $E_{bg} = 36.1\,\mathrm{kVcm}^{-1}$. Neumann conditions allow the electrons to flow out of the electrode and to form structures of high density around the electrode effectively stopping the simulation.

weights [1]. For the $36\,\mathrm{kVcm}^{-1}$ case in section 4.1 the average weight of the simulations is around 25, such that fluctuations are artificially increased by about a factor five. On the contrary, fluid models suppress dynamic fluctuations. Thus, PIC sets an upper bound and fluid models a lower bound to the discharge stochasticity. PIC with particle weight 1 would give correct fluctuations, but is not feasible due to the large number of particles required.

5.5. Streamer polarity and sources of free electrons

This work focused on negative streamers, which can propagate without nonlocal sources of free electrons, such as photoionisation or electron detachment. Photoionisation is an important mechanism for streamers in air, allowing positive streamers to propagate against the electron drift direction. The potential sources of free electrons in CO_2 with admixtures of CFN remain uncertain.

In [54, 55], photoionisation was implemented in pure CO_2. It was found that the weak photoionisation of CO_2 could sustain the propagation of positive streamers in sufficiently high background fields. There was however considerable uncertainty in the photoionisation parameters. Photoionisation in mixtures of CFN and CO_2 could be approximated by the photoionisation parameters for pure CO_2, but energetic photons might efficiently be absorbed by CFN. Such an effect was found in [56], where it was shown that adding CH_4 to air leads to a reduction in photoionisation.

Another source of free electrons could be electron detachment in a pre-ionized gas. Previous experimental work on swarm experiments shows evidence of detachment in CFN [57–59]. The detachment reactions are given in [58], and the detachment reaction rates in [57]. However, the presence and density of negative ions in front of the discharge remain uncertain and will depend in particular on the experimental conditions and the previous discharge history.

6. Conclusion and outlook

6.1. Conclusion

We first reviewed the transport and reaction coefficients in CO_2 with admixtures of CFN. The sensitivity of these coefficients to the choice of solver was analysed using BOLSIG+ and `particle_swarm` for different CFN-CO_2 mixtures. Both solvers produced similar μN, α/N, and η/N, while larger deviations were found for DN due to shortcomings of the two-term approximation [38]. Overall, both solvers are suitable.

Next, we compared particle_swarm results for transport and reaction coefficients with experimental data using different cross section sets at 1% and 10% CFN. Good agreement was obtained for μN and α_{eff}/N when using the Hayashi database for CO_2 combined with either the Flynn or Zhang datasets for CFN. Since these coefficients are the important inputs for fluid models, we chose the Hayashi set for CO_2 in our simulations. Different CFN cross sections had only a minor influence on the mixture coefficients, and we could not determine whether the Flynn or the Zhang set showed better agreement.

Finally, we investigated whether fluid models can model stochastic negative CFN-CO_2 streamers in various background fields. The fluid models approximate the particle model reasonably well, though branching occurred in particle simulations due to their intrinsic stochasticity. The particle model overestimates fluctuations due to the use of super-particles, whereas fluid models suppress them by averaging out fluctuations. Furthermore, with the LEA model streamers were generally the fastest.

6.2. Outlook

Combining modelling and experiments is essential for understanding the discharge behaviour and insulation performance of CFN-CO_2 mixtures. An essential next step is to validate the fluid and particle models for negative CFN-CO_2 streamers through experiments, as has been done for positive air streamers [60]. Such a validation enables the use of models to study the current open questions, such as:

(i) What are the generic properties of streamers that have strong attachment and little to no photoionisation?
(ii) Positive air streamers propagate more easily than negative streamers. Is this a generic streamer property, or will this be different for eco-friendly gases?

Another important step is to extend the fluid and particle models with processes such as photoionisation, detachment, and three-body reactions. However, reliable data must be obtained first. The CFN-CO_2 streamer structures are suspected to be highly stochastic, consisting of many smaller streamers. Therefore, computationally expensive 3D simulations are necessary. Developing reduced models as in e.g. [61, 62] might therefore be required.

Acknowledgments

The research of T S was supported by the Dutch Research Council (NWO) through the AES Project 20344 'Green Sparks'. The present study used the Dutch national e-infrastructure with the support of the SURF Cooperative using Grant Nos. EINF-10838 and EINF-10838.

Data availability statement

All data that support the findings of this study are included within the article (and any supplementary files).

Appendix A. Comparing CO_2 coefficients

The reduced transport and reaction coefficients are shown in figure A1 of the Hayashi [26], IST-Lisbon [31], Morgan [30], Phelps [29] and Triniti [28] CO_2 cross sections. The particle_swarm solver is used. The calculated coefficients have a clear division between the Hayashi and Morgan databases and the other databases for $\mu N, DN$ and η/N. We see this division less for α/N. Additionally, the values of the attachment rate η/N vary between the IST-Lisbon, Phelps, and Triniti databases, whereas the Hayashi and Morgan databases give quite similar η/N profiles.

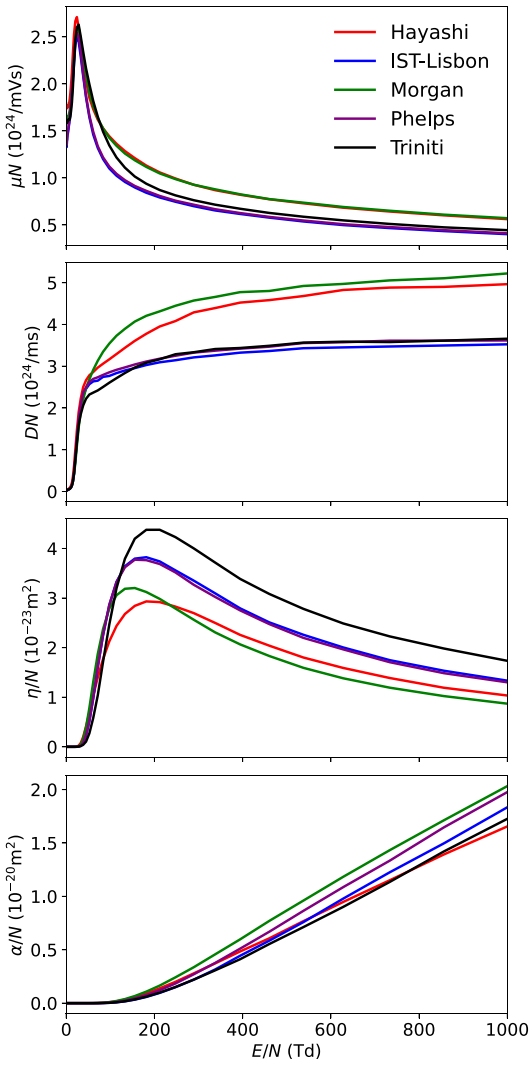

Figure A1. Comparison of the Hayashi, IST-Lisbon, Morgan, Phelps and Triniti reduced transport and reaction coefficients in pure CO_2 as function E/N. The coefficients are calculated with the particle_swarm code.

Appendix B. Numerical heating in particle-in-cell (PIC) simulations

In our PIC simulations the grid spacing Δx can exceed the Debye length

$$\lambda_D = \sqrt{\frac{\varepsilon_0 k_\mathrm{B} T_e}{n_\mathrm{e} e^2}}, \tag{B.1}$$

where k_B is Boltzmann's constant, T_e is the effective electron temperature and the contribution from ions has been ignored. Not resolving the Debye length can result in numerical heating and the thermalization of electrons, see e.g. [63]. However, these effects are usually not important when considering streamer discharges, as was recently studied in [64]. The main reason for this is that streamer discharges are weakly ionized. In the high-field region near the streamer head, the electron dynamics are driven by rapid energy and momentum gain from the field, balanced by rapid energy and momentum loss due to collisions, while numerical heating (or thermalization) will occur on a longer time scale. In the streamer channel there is a weaker field, but electrons will rapidly lose energy obtained from numerical heating in electron–neutral collisions. Only for very large ratios of $\Delta x/\lambda_D$ will numerical heating in the channel affect its conductivity. There will then be noise in the channel's electric field with an amplitude comparable to the critical field. However, since in the simulations presented here there was a rapid decay of channel electron density no such effects were visible.

As suggested by one of the referees, we have estimated the maximum ratio of $\Delta x/\lambda_D$. For the $36.1\,\mathrm{kVcm}^{-1}$ case, the maximum electron density at the streamer head is about $10^{20}\,\mathrm{m}^{-3}$, the grid

spacing is about $\Delta x = 5\,\mu$m and the effective electron temperature is about $T_e \sim \frac{2}{3}\,(6\,\mathrm{eV}/k_B)$. This results in a ratio $\Delta x/\lambda_D \sim 3$. Further back in the channel the mesh is a factor two larger but the electron density is lower, so we still have $\Delta x/\lambda_D \sim 3$. We have made similar estimates for the $34.2\,\mathrm{kVcm}^{-1}$ and $38.2\,\mathrm{kVcm}^{-1}$ cases, and found a maximum ratio of $\Delta x/\lambda_D \sim 4$. With these values effects due to numerical heating are expected to be negligible [64].

ORCID iDs

Thomas J G Smits 0009-0005-2605-4562
Jannis Teunissen 0000-0003-0811-5091
Ute Ebert 0000-0003-3891-6869

References

[1] Nijdam S, Teunissen J and Ebert U 2020 *Plasma Sources Sci. Technol.* **29** 103001
[2] Rabie M and Franck C M 2018 *Environ. Sci. Technol.* **52** 369–80
[3] Intergovernmental Panel on Climate Change 2021 *Climate Change 2021: The Physical Science Basis. Contribution of Working Group I to the Sixth Assessment Report of the Intergovernmental Panel on Climate Change* (Cambridge University Press)
[4] Global warming potentials (IPCC second assessment report) UNFCCC website accessed: 2025-06-16; includes GWP values for key greenhouse gases (available at: https://unfccc.int/process/transparency-and-reporting/greenhouse-gas-data/greenhouse-gas-data-unfccc/global-warming-potentials)
[5] Skirbekk F, Mauseth F and Meyer H K H 2022 Pre-breakdown phenomena in technical air with and without c5-fluoroketone for a rod-plane gap *Proc. Nordic Insulation Symp.* vol 27
[6] Guo B, Ebert U and Teunissen J 2023 *Plasma Sources Sci. Technol.* **32** 115001
[7] Vemulapalli H, Meyer H K H, Mauseth F and Franck C M 2024 Measurement of streamer radii in sf 6 alternatives: Mixtures of Co_2/O_2 and $C_4\,F_7N$ in Co_2/O_2 *2024 IEEE Conf. on Electrical Insulation and Dielectric Phenomena (CEIDP)* (IEEE) (https://doi.org/10.1109/CEIDP61745.2024.10907615)
[8] Seeger M, Avaheden J, Pancheshnyi S and Votteler T 2016 *J. Phys. D: Appl. Phys.* **50** 015207
[9] Yan X, Zhou X, Li Z, Qian Y and Sheng G 2023 *Appl. Sci.* **13** 1409
[10] Vu-Cong T, Toigo C, Ortiz G, Dalstein M, Jacquier F and Girodet A 2020 Numerical simulation of partial discharge current pulse: Comparison between sf6, fluoronitrile-co2 mixture and fluoroketone-co2 mixture *2020 IEEE Conf. on Electrical Insulation and Dielectric Phenomena (CEIDP)* (IEEE) (https://doi.org/10.1109/CEIDP49254.2020.9437474)
[11] Yan X, Zhou X, Li Z, Qian Y and Sheng G 2023 *AIP Adv.* **13** 035238
[12] Fan B, Zhou X, Qian Y and Zang Y 2022 Simulation of positive surface discharge in c4f7n gas mixture *2022 7th Asia Conf. on Power and Electrical Engineering (ACPEE)* (IEEE)
[13] Gao Q, Wang X, Adamiak K, Qi X, Yang A, Liu D, Niu C and Zhang J 2022 *AIP Adv.* **12** 095101
[14] Wang F, Wang L, Chen S, Sun Q, Zhong L and Zhuang C 2021 *IEEE Trans. Plasma Sci.* **49** 2048–54
[15] Grubert G, Becker M and Loffhagen D 2009 *Phys. Rev. E* **80** 036405
[16] Dias T C and Guerra V 2025 *J. Appl. Phys.* **58** 185204
[17] Dujko S, Markosyan A, White R and Ebert U 2013 *J. Phys. D: Appl. Phys.* **46** 475202
[18] Markosyan A H, Teunissen J, Dujko S and Ebert U 2015 *Plasma Sources Sci. Technol.* **24** 065002
[19] Levko D, Thiruppathiraj S and Raja L L 2024 *J. Appl. Phys.* **135** 173301
[20] CIGRÉ Working Group A341 2022 Current interruption in SF_6-free Switchgear *Technical Brochure* 871 (International Council on Large Electric Systems (CIGRÉ))
[21] Pancheshnyi S, Biagi S, Bordage M C, Hagelaar G, Morgan W, Phelps A and Pitchford L C 2012 *Chem. Phys.* **398** 148–53
[22] Carbone E, Graef W, Hagelaar G, Boer D, Hopkins M M, Stephens J C, Yee B T, Pancheshnyi S, Van Dijk J and Pitchford L 2021 *Atoms* **9** 16
[23] Pitchford L C *et al* 2017 *Plasma Process. Polymers* **14** 1600098
[24] Flynn M, Agan J, Neuber A and Stephens J 2023 *J. Phys. D: Appl. Phys.* **56** 485207
[25] Zhang B, Hao M, Yao Y, Xiong J, Li X, Murphy A B, Sinha N, Antony B and Ambalampitiya H B 2023 *J. Phys. D: Appl. Phys.* **56** 134001
[26] Hayashi database (available at: www.lxcat.net) (Accessed 31 May 2024)
[27] Hayashi M 1992 *Plasma Material Science Handbook* 748
[28] Triniti database (available at: www.lxcat.net) (Accessed 25 June 2024)
[29] Phelps database (available at: www.lxcat.net) (Accessed 31 May 2024)
[30] Morgan database (available at: www.lxcat.net) (Accessed 27 June 2024)
[31] Ist-lisbon database (available at: www.lxcat.net) (Accessed 31 May 2024)
[32] Alves L 2014 The ist-lisbon database on lxcat *J. Phys.: Conf. Ser.* **565** 012007
[33] Hagelaar G and Pitchford L C 2005 *Plasma Sources Sci. Technol.* **14** 722
[34] Teunissen J, Rutjes C, Bouwman D, Li X and Martinez A 2025 MD-CWI/particle_swarm: First release *Zenodo*
[35] Martinez N A 2022 Computational Investigations of Streamers: From Input Cross Sections to Evolution of Plasma Species *Phd Thesis* p 1 (research tu/e / graduation tu/e) Applied Physics and Science Education proefschrift
[36] Petrović Z L, Dujko S, Marić D, Malović G, Nikitović Ž, Šašić O, Jovanović J, Stojanović V and Radmilović-Radjenović M 2009 *J. Phys. D: Appl. Phys.* **42** 194002
[37] Stephens J 2018 *J. Phys. D: Appl. Phys.* **51** 125203
[38] Hagelaar G 2025 *Phys. Plasmas* **32** 043501
[39] Zhang B, Xiong J, Hao M, Yao Y, Li X and Murphy A B 2022 *J. Appl. Phys.* **131** 033304
[40] Chachereau A, Hösl A and Franck C M 2018 *J. Phys. D: Appl. Phys.* **51** 495201
[41] Vemulapalli H and Franck C M 2023 *J. Appl. Phys.* **56** 065202
[42] Li C, Brok W, Ebert U and Van der Mullen J 2007 *J. Appl. Phys.* **101** 064505

[43] Petrović Z L, Šuvakov M, Nikitović Ž, Dujko S, Šašić O, Jovanović J, Malović G and Stojanović V 2007 *Plasma Sources Sci. Technol.* **16** S1
[44] Teunissen J and Ebert U 2018 *Comput. Phys. Commun.* **233** 156–66
[45] Teunissen J and Ebert U 2017 *J. Phys. D: Appl. Phys.* **50** 474001
[46] Soloviev V R and Krivtsov V M 2009 *J. Phys. D: Appl. Phys.* **42** 125208
[47] Teunissen J 2020 *Plasma Sources Sci. Technol.* **29** 015010
[48] Teunissen H and Ebert U 2016 *Plasma Sources Sci. Technol.* **25** 044005
[49] Vahedi V and Surendra M 1995 *Comput. Phys. Commun.* **87** 179–98
[50] Boeuf J P and Marode E 1982 *J. Phys. D: Appl. Phys.* **15** 2169
[51] Wang Z, Sun A and Teunissen J 2022 *Plasma Sources Sci. Technol.* **31** 015012
[52] Childs H *et al* 2011 *Proceed SciDAC* pp 1–16
[53] Levko D and Raja L 2023 *J. Appl. Phys.* **133** 053301
[54] Marskar R 2024 *Plasma Sources Sci. Technol.* **33** 025023
[55] Li X, Dijcks S, Sun A, Nijdam S and Teunissen J 2024 *Plasma Sources Sci. Technol.* **33** 095009
[56] Bouwman D, Teunissen J and Ebert U 2022 *Plasma Sources Sci. Technol.* **31** 045023
[57] Hösl A, Chachereau A, Pachin J and Franck C M 2019 *J. Phys. D: Appl. Phys.* **52** 235201
[58] Ranković M, Kumar T P, Nag R, Kočišek P J and Fedor J 2020 *J. Chem. Phys.* **152** 244304
[59] Mirpour S and Nijdam S 2022 *Plasma Sources Sci. Technol.* **31** 055007
[60] Li X, Dijcks S, Nijdam S, Sun A, Ebert U and Teunissen J 2021 *Plasma Sources Sci. Technol.* **30** 095002
[61] Teunissen J and Malagón-Romero A 2025 *Comput. Phys. Commun.* **315** 109733
[62] Luque A and Ebert U 2014 *New J. Phys.* **16** 013039
[63] Jubin S, Powis A T, Villafana W, Sydorenko D, Rauf S, Khrabrov A V, Sarwar S and Kaganovich I D 2024 *Phys. Plasmas* **31** 023902
[64] Nikic D, Fierro A, Moore C H and Lehr J 2026 *Plasma Sources Sci. Technol.* **35** 025017